CrossMark

ORIGINAL PAPER

Ultrasensitive direct detection of dsDNA using a glassy carbon electrode modified with thionin-functionalized multiple graphene aerogel and gold nanostars

Li Ruiyi[1] · Wang Jiajia[1] · Liu Ling[1] · Li Zaijun[1,2]

Abstract The paper reports on the synthesis of a composite consisting of thionin-functionalized multiple graphene aerogel and gold nanostars (termed TF-MGA/GNSs). The composite displays an enhanced electrochemical performance compared to the classical graphene aerogel. The performance can be further improved by increasing number of the graphene oxide gelation cycles. The composite was deposited on a glassy carbon electrode to obtain a biosensor for the direct detection of dsDNA. The interaction of thionin with dsDNA causes a specific electrochemical response, best at a working voltage of −228 mV (vs. Ag/AgCl). The enhanced electrocatalytic activity of the composite strongly improves sensitivity. The differential pulse voltammetric signal linearly decreases with increasing dsDNA concentration in the range from 100 fg·mL^{-1} to 10 ng·mL^{-1}, and the detection limit is 39 fg·mL^{-1} (at an S/N ratio of 3). The method is sensitive, selective and rapid. It was successfully applied to the detection of circulating free DNA in human serum. The study also provides an attractive approach towards graphene aerogel-based materials to meet the needs of nanoelectronics for molecule diagnosis, bioanalysis and catalysis.

✉ Li Zaijun
zaijunli@263.net

1 School of Chemical and Material Engineering, Jiangnan University, Wuxi 214122, China

2 Key Laboratory of Food Colloids and Biotechnology, Ministry of Education, Wuxi 214122, China

Introduction

The sensitive and selective detection of DNA has become a subject of intense research due to its potential applications in the fields of pharmacogenetics, pathology, genetics and food safety [1]. Analytical techniques for detection of DNA include spectrophotometry [2], fluorescence [3], surface enhanced Raman scattering [4], chemoluminescence [5] and electrochemical methods [6]. Among them, electrochemical DNA biosensors are attractive on account of their high sensitivity and selectivity, portability, rapid response and low cost. Nanomaterials such as graphene [7], carbon nanotubes [8] and gold nanoparticles [9] have been used to construct electrochemical DNA sensors owing to their good electrical properties and large specific surface areas. But so far most of the reported DNA sensors were applied to the detection of selected DNA sequences. Few studies on the electrochemical detection of double-stranded DNA (dsDNA) are reported. In fact, DNA is rarely present in single-stranded form, either naturally or after PCR amplification. The improvements in the detection of dsDNA or natural DNA leads to more robust and flexible DNA diagnostics [10].

Graphene has been widely applied in fields such as sensing [11], solar cells [12], electrocatalysis [13], supercapacitors [14] and lithium ion batteries [15]. Compared to the two-dimensional graphene powder, graphene aerogel (GA) possesses a much higher electrical conductivity since the constituent graphene sheets are chemically bonded, facilitating much faster charge transport across graphene sheet junctions, a high specific surface area that offers abundant active sites for the catalytic

reduction events, and large pore volume that provides fast mass transfer of the redox species [16–20]. Three main ways have been successfully developed for building on the GA-based materials to further improve the electrochemical properties. One way is to use small molecular as crosslinking agent to connect graphene sheets into a whole structure. The resulting GA holds low electrical resistance and good compressibility [21]. Another way is to use a specific conducting polymer to improve the electrical conductivity [22]. The investigation confirms that the introduction of conducting polymer largely enhances the electrical conductivity [23]. Certain polymers have been applied to enhance the mechanical strength of GA. The resulting GA exhibit excellent mechanical property, high electrical conductivity and light weight. However, the use of above ways only leads to ultralight GA due to the low water-solubility of graphite oxide. The ultralight characteristic inevitably results in a relatively poor mechanical strength and electrical conductivity owing to sparse graphene sheets and fragile frame structure. This will limit its application in the detection of DNA which requires an ultra high sensitivity.

Herein, we report on the synthesis of a composite consisting of thionin-functionalized multiple graphene aerogel and gold nanostars (termed TF-MGA/GNSs) and its use as an electrochemical sensing platform for the direct detection of DNA. The result reveals that the MGA displays a much better electrocatalytic activity compared to the classical GA. Since significant synergy between MGA and GNS was achieved, the electrochemical sensor based on the TF-MGA/GNSs provides the advantage of sensitivity and rapidity. The method was successfully applied to the detection of circulating free DNA in human serum.

Experimental

Materials and reagents

Chlorauric acid ($HAuCl_4$), silver nitrate ($AgNO_3$), thionin and bovine serum albumin (BSA) were purchased from Sigma-Aldrich (http://www.sigmaaldrich.com/china-mainland.html). Deoxyribonucleic acid (dsDNA) sodium salt from salmon sperm with molecular weight of 50–100 kDa was bought from Acros Organics (acros.com). The concentration of standard DNA stock solution was spectrophotometrically determined by measuring the absorbance of the diluted solution at 260 nm. DNA was extracted from human serum by using a circulating nucleic acid kit purchased from CWbiotech (www.cwbiotech.com). Briefly, protease was used to degrade the protein in the serum. Then, the ionic strength of the solution was enhanced and an adsorption column was used to extract DNA from the mixture. Graphite oxide

(GO) was prepared from natural graphite by Hummers' method [24]. The 24-base oligonucleotide (ssDNA-1, 5′-ACC AAG TCA TCA GCA GCC ACG GAA-3′) and 36-base oligonucleotide (ssDNA-2,5′-GCG AGG TTC CGT GGC TGC TGA TGA CTT GGT CCT CGC-3′) were synthesized by Shanghai Sangon Biotechnology Co. Ltd. (www.sangon.com). The thionin solution was prepared by dissolving thionin in ethanol with a concentration of 10 mg mL^{-1}. Phosphate-buffered saline (PBS, pH 7, Na_2HPO_4-KH_2PO_4-NaCl-KCl, 0.01 M) was prepared. The chitosan solution was prepared by dissolving 5.0 g chitosan in 100 mL of 1.0 % (v/v) acetic acid. All other reagents employed were of analytical reagent grade or with the highest quality and were purchased from Shanghai Chemical Company (www.alibaba.com/showroom/shanghai-chemical-company-ltd.html). Ultra pure water (18.2 MΩ cm) purified from a Milli-Q purification system was used throughout the experiment.

General characterization

Scanning electron microscopy (SEM) was carried out with a Hitachi S4800 field emission scanning electron microscope. SEM sample was prepared by placing a drop of dilute ethanol dispersion of the composites onto a copper plate attached to an aluminum sample holder, and the solvent was allowed to evaporate at room temperature. Transmission electron microscope (TEM) images were acquired with a JEOL 2010 transmission electron microscope at 200 keV. The sample was prepared by dispensing a small amount of dry powder in ethanol. Then, one drop of the suspension was dropped on 300 mesh copper. TEM grids covered with thin amorphous carbon films. The X-ray diffraction (XRD) pattern was measured on a X-ray D8 Advance Instrument operated at 40 kV and 20 mA and using Cu Kα radiation source with λ = 0.15406 nm. Infrared spectrum (IR) was recorded on a Nicolet FT-IR 6700 spectrometer. The absorbance and absorption spectra were recorded with a TU-1901 spectrophotometer.

Preparation of the gold nanostars (GNSs)

The $HAuCl_4$ solution (10 mL, 4 mg mL^{-1}) was mixed with the citrate acid solution (5 ml, 30 mg mL^{-1}) and the tannic acid solution (5 mL, 1.0 mg mL^{-1}). To prepare the gold seed solution, the mixed solution was heated at 70 °C until the color of the solution became clear crimson, then quickedly increased up to the temperature of 100 °C, stayed for 5 min at the temperature and cool the solution to room temperature.

Ultrapure water (2.5 mL) was transferred into another clean flask. Citric acid solution (0.05 M, 25 μL) was then dropped into the $HAuCl_4$ solution (0.03 M, 50 μL) under

stirring. The solution was incubated for 5 min at room temperature. This was followed by adding the $AgNO_3$ solution (0.01 M, 30 μL) under stirring. As soon as hydrogen peroxide (30 %, 2.5 mL) was poured into the solution, the gold seed solution (10 μL) was rapidly injected and stirred for 30 s to obtain the GNS solution.

The composite synthesis

The synthesis of MGA includes four processes. In a typical procedure, the GO dispersion was made by GO (0.2 g) with ascorbic acid (0.6 g) in ultrapure water (50 mL), and refined by ultrasonic condition to form homogeneous GO dispersion. The dispersion was heated at 40 °C and allowed to stand for 16 h to form graphene hydrogel. The hydrogel was treated by freeze-drying to produce GA. Next, prick holes on the top of the GA with 1 mm steel needles. Place the GA into a volumetric glass vial with a cover to keep the inner volume fitting the shape of the GA, and then add the GO dispersion with the same scale (GO/ascorbic acid = 1:3) of 30 mL into the GA via the small holes. The vial was put into the water bath (40 °C) for 16 h for the second GO gelation. The MGA-1 was obtained by freeze drying. Next, repeat the operation in the second process until number of the GO gelation cycle reaches a desired value. Finally, the MGA was annealed at 800 °C in Ar/H_2 (95 : 5) for 2 h. Based on number (n) of the GO gelation cycle during the synthesis, the corresponding product is designated as MGA-n.

A fraction of MGA-n (10 mg) was dispersed into ultrapure water (10 mL) by ultrasonic treatment for 12 h to form a stable suspension. Then, it was mixed with the GNSs solution by the volume ratio of 1:1. For sufficient contact and hybridize, the mixture was ultrasonicated for 6 h. Finally, the thionin solution (0.5 mL) was dropwise added and the solution ultrasonicated for another 6 h. Finally, it was dried by freeze drying to obtain TF-MGA-n/GNSs.

Sensor fabrication

Glassy carbon electrode (GCE, 1.0 mm in diameter) was polished successively with 1.0, 0.3, and 0.05 μm alumina powder, and sonicated in a 6.0 M of nitric acid/doubly distilled water and ethanol/doubly distilled water for 20 min. The GCE was subjected to cyclic scanning in 0.5 M of sulphuric acid solution in a potential range from −0.1 to 1.0 V. When the cyclic voltammogram was almost unchanged, the electrode was taken out, cleaned with ultra pure water and finally dried in a stream of nitrogen. The treated GCE was modified with different graphene material to prepare different sensor using the following procedure: the amounts of TF-MGA-n/GNSs was dispersed in 1.0 % chitosan solution to make up 0.2 mg mL^{-1} dispersion. Then, 10 μL of the dispersion was

dropped on the surface of GCE and dried in air. The above procedure was repeated two times to obtain the sensor.

Electrochemical measurements

Electrochemical measurements were performed with a CHI660D electrochemical workstation (Shanghai, China). Conventional three electrode system was used for cyclic voltammetry (CV) with Ag/AgCl (saturated KCl) electrode as the reference electrode, platinum wire as the counter electrode, and bare or modified GCE electrode as the working electrode. The electrochemical experiment was carried out under room temperature, and all experimental solution was degassed by nitrogen for at least 15 min. Then, a nitrogen atmosphere was maintained during electrochemical measurements. The cyclic voltammograms (CVs) and differential pulse voltammograms (DPVs) were recorded in the PBS containing different concentration of dsDNA. The reported result for every electrode was the mean value of five parallel measurements.
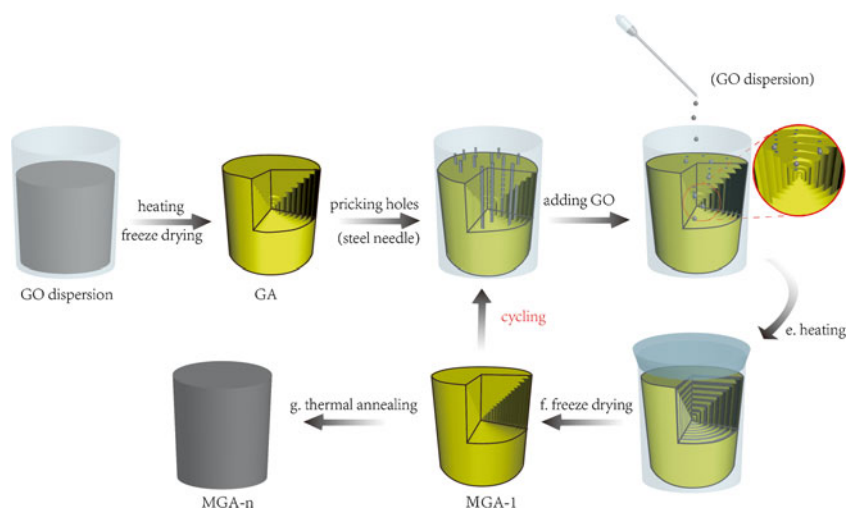
Results and discussion

Synthesis and characterization

The synthesis of MGA-n includes four assemble processes (shown in Fig. 1). The first process is to prepare GA. Firstly, GO and ascorbic acid were dispersed in ultrapure water by the ultrasonication to form a homogeneous GO dispersion. Then, the dispersion was heated to produce graphene hydrogel. During the process, GO sheets were partly reduced and self-assembled into graphene hydrogel. To reduce the temperature for the formation of graphene hydrogel, ascorbic acid was used as an effective agent for reducing GO sheets. The result shows that the GO dispersion turned to black when heated at 40 °C for 0.5 h in the presence of ascorbic acid. After being heated for 1 h, a black monolith formed and slightly floated up to the top of the vial. This is because the hydrophobic reduced GO tends to self-assemble into three-dimensional macroscopic structure through p-interaction and finally forms a grapheme hydrogel. Finally, the graphene hydrogel was dried by freeze-drying to obtain GA. Due to slow evaporation of water, high mechanical strength and three-dimensional structure of the graphene hydrogel can be well maintained during the drying.

The second process is to synthesize double GA (termed MGA-1). Firstly, prick holes on the top of the GA with steel needles. This is significant to produce MGA due to the closure and hydrophobic properties of GA. The formed small holes not only open the smooth and dense surface for dredging, but also effectively resolve the difficulty that the GO dispersion

Fig. 1 Procedure for the synthesis of MGA

The density and resistance of MGA-n samples with different number of the GO gelation cycle are presented in Fig. S1. Fig. S1A shows that the density of MGA-n rapidly increases with increasing number of the GO gelation cycles. For the synthesis of MGA-n, new graphene framework was formed in situ in the old graphene framework during each of the GO gelation. The new framework and the old framework intertwines each other to form a whole network structure. This make the graphene network become more dense and robust with increasing number of the GO gelation cycle. Compared to the MGA-n with a smaller n value, the MGA-n with a bigger n value displays a smaller and denser pore structure with a narrower pore size distribution. As the graphene sheet itself is of good electrical property, to increase the density is one of most simple and effective methods for improving its electrical conductivity. This conclusion has been confirmed by the results of resistance measurement in Fig. S1B.

entering into the interior of GA. Since steel needles break the barrier between the adjacent closed pores to form plenty of open holes. Those holes were grouped and worked as channels to connect all the gaps in the GA. Based on these, the volume of the GO dispersion that can reach the interior of GA will largely increase. For the synthesis of MGA-n, the increase in the density for each GO gelation cycle depends on the volume of the GO dispersion that entered into the interior of GA, a big volume of GO dispersion will lead to a big increase in the density of GA. However, the number of the holes is not unlimited. The excessive pricking holes may lead to the facial failure of GA. In our experience, the number of the holes above 5 per square centimeter was in excess. Then, place the GA into another vial with a cover. The vial was not chosen at random, but was designed to fit the shape of the GA. The inner volume of the vial exactly meets with the GA, and ideally has no gap between the vial wall and GA. A suitable cover is also necessary to fix the GA inside of the vial. Next, the GO dispersion was dropped into the GA via those small holes. Here, drip tube rather than vial was used because direct pouring may damage the surface of the GA. After the GO dispersion filled the GA, put the vial into the water-bath for heating to form double graphene hydrogel. Although the GO dispersion inside of the GA will expand during the heating process, the specially-made vial prevents the increase of the GA volume and exhibits a maximum density enhancement of GA. Finally, the double graphene hydrogel was treated by freeze-drying to obtain double GA (termed MGA-1).

The third process is to prepare MGA-n ($n > 1$). The MGA-n was made from MGA-1 by repeating the second process until cycling number of the GO gelation reaches a desired value. The fourth process is to reduce MGA-n by thermal annealing in Ar/H$_2$. The reduction treatment further strips the oxygen containing groups in the MGA-n and leads to an enhanced electrical conductivity.

Figure 2 presents typical SEM, high-resolution TEM (HRTEM) and SAED images of the MGA-5. The MGA-5 displays a three-dimensional architecture with well-defined porous structure, suggesting efficient assembly of GO sheets during the hydrothermal reaction. The HRTEM analysis further reveals the crystallinity of MGA-5. The lattice spacing of 0.22 nm agrees with that of in-plane lattice spacing of graphene. On the SAED image several hexagonal diffraction geometry of graphene is clearly shown on the electron diffraction patterns, and no direction is extended to the ring. In addition, the most inner layer (100) diffraction ring is obviously stronger than the secondary inner layer (110) diffraction ring, verifying that the graphene layer in the selected regions is very thin [25].

The GNSs solution was added into the MGA suspension by the ratio of 1:1 for the hybridization with GNSs. The GNSs were sufficient adsorbed on the MGA surface during the process. The formed MGA-5/GNSs composite was characterized by TEM and XRD. Figure 3a shows that the GNS offers an

Fig. 2 SEM (**a**), HRTEM (**b**) and SAED images (Inset in **b**) of MGA-5
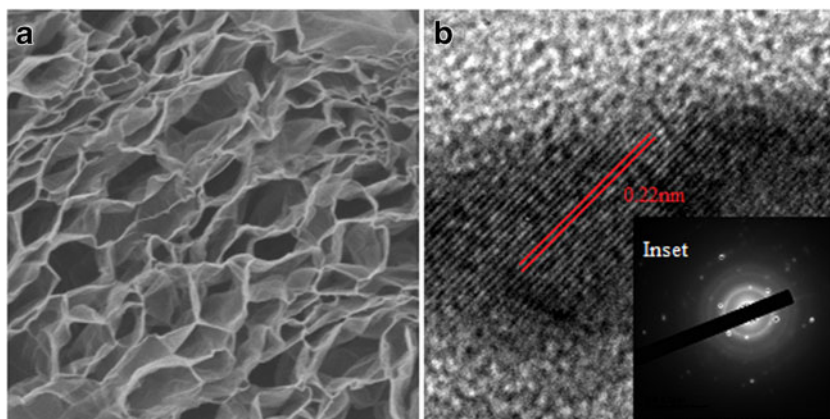

unique structure with rod-like spikes randomly protruding outwards. Compared to the gold nanoparticles with a smooth and flat surface, the gold nanocrystals with sharp edges and tips can offer a stronger localized surface plasmon resonance, leading to a better electrocatalytic activity to thionin. On the XRD patterns in Fig. 3b there are five diffraction peaks at scattering angles of 26°, 38.28°, 44.48°, 64.6° and 77.64°. The strong diffraction peak at 26° is assigned to graphene, corresponding to the crystal plane graphene (100). Often, graphene gives a weak and wide diffraction peak at 26° due to low degree of crystallization. The peaks at 38.28°, 44.48°, 64.6° and 77.64° are assigned to GNSs, corresponding to the crystal planes Au (111), Au (200), Au (220) and Au (311) of gold face-centered cubic crystallographic structure (JCPDS card No. 65-2870).

The thionin solution (0.5 mL) was mixed with the MGA/GNSs and then was dried by freeze drying to obtain TF-MGA/GNSs. The IR spectrum of TF-MGA/GNSs is presented in Fig. S2. On the IR spectrum there are many IR absorption peaks. These IR absorption peaks are attributed to the thionin on the composite, which are similar with that of sole thionin. The result confirms that that the MGA/GNSs has been successfully functionalized by thionin.

Electrochemical studies

Cyclic voltammetric (CV) performance of the electrodes modified with different sensing material was investigated in the PBS (pH 7) to understand the electrochemical properties. The results are shown in Fig. 4. It can be seen that all CV curves offer a pair of reversible redox peaks. These are attributed to oxidation-reduction process of the thionin on the electrode surface. Compared to the electrode modified with TF-MGA-1, the electrode modified with TF-MGA-5 gives a much higher peak current. The better electrical conductivity and well-defined porous structure of TF-MGA-5 achieve to a faster electron transfer and mass transport during the electrode reaction, leading to a higher electrocatalytic activity. After the GNSs were introduced into the MGA, the peak current further increases. This is because gold nanomaterials act as the artificial enzyme with highly electrocatalytic activity [26]. Since the GNS is of a rich of sharp edges and tips, which brings a strong localized surface plasmon resonance [27], it can offer a much higher electrocatalytic activity compared to the gold nanospheres and the gold nanorods. Such a specific electrocatalytic activity will result in an obviously enhanced electrochemical response to thionin. The synergy of MGA and GNS

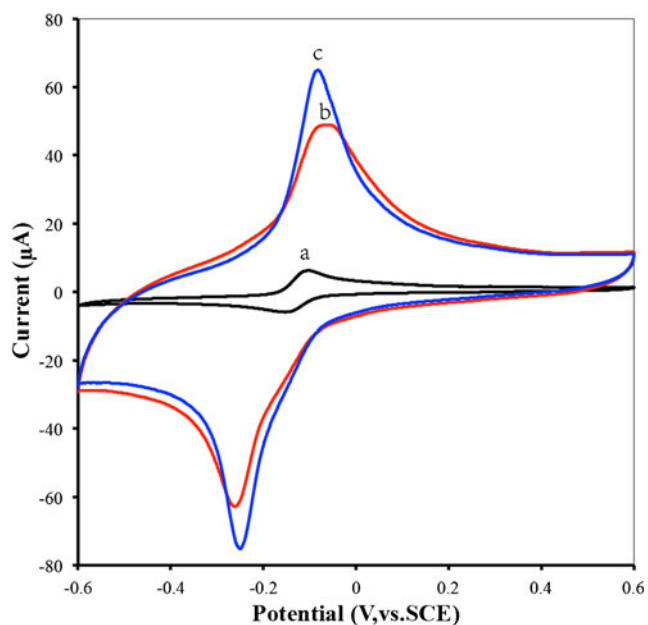**Fig. 3** TEM image (**a**) and XRD patterns (**b**) of MGA-5/GNSs
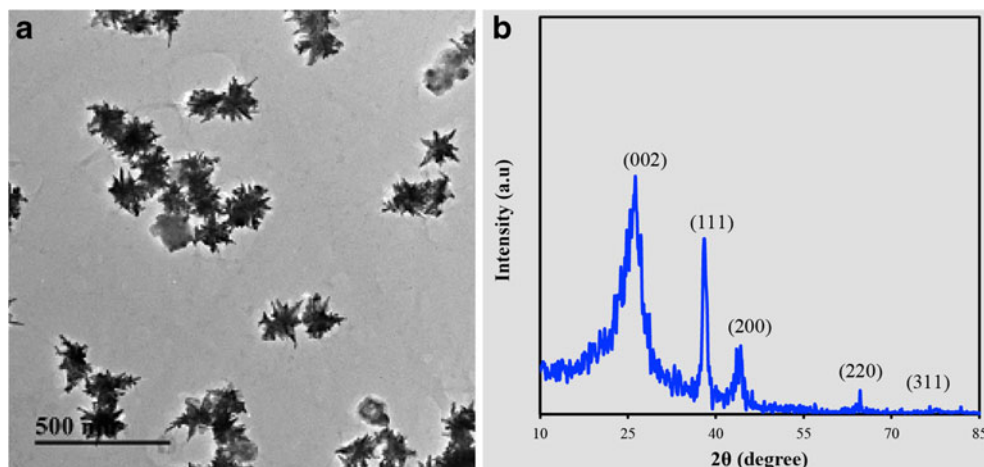
Fig. 4 CV curves of TF-MGA-1 sensor (**a**), TF-MGA-5 sensor (**b**) and TF-MGA-5/GNSs sensor (**c**) in the PBS (pH 7) at the scan rate of 100 mV s^{-1}

in the electrocatalytic performance greatly increases the peak current and the improve the sensitivity to DNA.

Electrochemical response to dsDNA

Fig. S3 presents the CV curves of TF-MGA-1 sensor, TF-MGA-5 sensor and TF-MGA-5/GNSs sensor in the absence and the presence of dsDNA (1.0 pg mL^{-1}) in the PBS (pH 7). Thionin was used as a redox probe for the detection of dsDNA. Thionin is a kind of cationic phenothiazine dye that can show electrochemical activity, thus all sensors offer a pair of the redox peaks on the CV curve. In addition, thionin can bind with dsDNA through the intercalation and electrostatic interaction to form stable complex. The complex will partially block the channels of the electron transfer and mass transport between the electrode and the electrolyte, leading to a slower redox reaction process. Thus, the introduction of dsDNA will lead to a reduced peak current for the each sensor. In the study, MGA-1, MGA-5 or MGA-5/GNSs was used as a sensing material for improving the electrochemical activity to thionin. Fig. S3 shows that the peak current change (ΔI) before and after added dsDNA for different sensors exists an obvious difference. Among three sensors, the TF-MGA-5/GNSs sensor provides the biggest peak current change after introduced dsDNA among three sensors. Its ΔI value is more than 12-fold that of the TF-MGA-1 sensor, indicating the most sensitive electrochemical response to dsDNA. This is attributed to the excellent electrocatalytic activity of MGA-5/GNSs, which improves the redox reaction process of thionin and leads to an

enhanced peak current response. This help to increase the sensitivity for the detection of DNA.

The reaction kinetics of TF-MGA-5/GNSs sensor in the presence of dsDNA (1.0 pg mL^{-1}) in a pH 7 of the PBS were studied. The CV curves of the TF-MGA-5/GNSs sensor at different scan rates are presented in Fig. S4A. All scan rates resulted in well-defined reduction and oxidation peaks with little shift in both cathodic and anodic peak potentials with respect to scan rate in the presence of dsDNA. Both its cathodic and anodic peak currents are linearly increase with the increase of scan rate (see Fig. S4B), indicating that the electrode reaction corresponds to the solution phase is a quasi-reversible process. Besides, the electrochemical response of the composite is quite stable. Only a slight decrease in current is observed for the composite after continuous scanning for 50 cycles (not shown).

Analytical characteristics

The TF-MGA-5/GNSs sensor was used to determine the concentration of the natural dsDNA based on the interaction of thionin and dsDNA. The differential pulse voltammetry (DPV) was chosen to record the current response of the electrode because it is much more sensitive than CV. Figure 5a presents the DPV curves of the sensor in the PBS (pH 7) without and with the successive injection of dsDNA. The thionin showed an oxidization peak at −228 mV vs. Ag/AgCl on the DPV curves. The peak current decreases with the increase of the dsDNA concentration due to the electrostatic interaction and intercalation of thionin with dsDNA. Furthermore, the peak current from those curves shows a linear relationship with the logarithm value of the dsDNA concentration in the range from 100 fg mL^{-1} to 10 ng mL^{-1}. The corresponding linear regression equation was fitted as: $I_p = -0.6967 \log C + 23.148$, and the statistically significant correlation coefficient was 0.9978. Within the two quantities in the equation, I_p is the intensity of peak current in μA and C is the logarithm value of dsDNA concentration, which is in the unit of g mL^{-1}. The detection limit is 39 fg mL^{-1} for the dsDNA that was obtained from the signal-to-noise characteristics of these data (at an S/N ratio of 3). The sensitivity is much better than that of the reported electrochemical DNA biosensors for the direct detection of dsDNA in Table 1.

The reproducibility of this dsDNA sensor is acceptable. Its relative standard deviation (RSD) is 3.7 % for six replicate preparations and measurements at the concentration of 1.0 ng mL^{-1}. What is more, the responses of this sensor are nearly the same for six successive measurements. This indicates that the sensor is effective for sensitive and accurate detection of dsDNA. However, its long-term stability is inferior. After it is incubated in the PBS for 24 h, its response currents decrease and its redox potentials shift due to the

Fig. 5 **a** DPV curves of TF-MGA-5/GNSs sensor in the PBS (pH7.0) containing 1.0×10^{-13}, 3.0×10^{-13}, 1.0×10^{-12}, 3.0×10^{-12}, 1.0×10^{-11}, 3×10^{-11}, 1.0×10^{-10}, 3.0×10^{-10}, 1.0×10^{-9}, 3.0×10^{-9} and 1.0×10^{-8} g mL^{-1} of dsDNA (from *top* to *down*). **b** Calibration plots of the concentration of dsDNA vs. peak current change (DIp). The DPV parameters were set to a scan rate of 4 mV s^{-1}, 50 mV pulse amplitude, 20 ms pulse width and -0.2 V initial potential
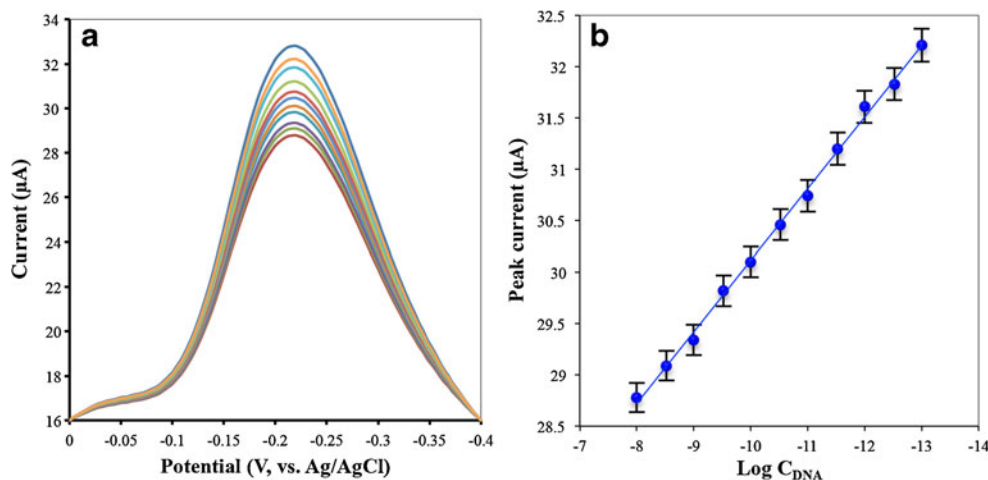
swelling of the modified film, resulting in falling off partially from the electrode surface.

The TF-MGA-5/GNSs sensor also shows sensitive response to ssDNA, because ssDNA can be dyed by thionin. Fig. S5 shows the DPV curves of the sensor in the absence and the presence of 1×10^{-10} M of the ssDNA-1 and 1×10^{-10} M of the ssDNA-2. The result shows that both ssDNA-1 and ssDNA-2 can cause an obvious decrease of the DPV signal. The detection limit is 2.2×10^{-13} M for the ssDNA-1 and 1.6×10^{-13} M for the ssDNA-2. Therefore, the constructed sensor is applicable to the direct detection of ssDNA by the electrochemical method.

Comparison of different materials

The good sensitivity of this sensor is attributed to the electro-catalytic activity of MGA-n and GNSs. Previous research indicates that MGA-n can offer an enhanced electrochemical performance compared to the classical GA. The performance can be further improved by increasing number of GO gelation cycles. The introduction of GNSs achieves to more sensitive and selective detection of dsDNA due to good electrical property and large specific surface area. To quantitatively evaluate the effect of the MGA-n with different n and GNSs on the sensitivity, a series of sensors were designed, fabricated and used for the electrochemical detection of dsDNA by the DPV method. Their linear range and detection limit were shown in Table 2. Three conclusions can be drawn from Table 2. First conclusion is that the TF-MGA-n/GNSs sensor with a higher n value can offer a higher sensitivity, indicating a better the electro-catalytic activity to thionin. This is because a bigger n will bring a better electrical conductivity and more stable porous structure, which will greatly improve the electron transfer and electrolyte transport during the catalyzing process, and results in more sensitive electrochemical response. The fact also proves that increasing the number of GO gelation cycle is one of the most effective methods to improve the sensitivity. Second conclusion is that GNS is of high electro-catalytic activity to thionin. Often The GNS acts as an artificial enzyme to selectively catalyze the oxidation and reduction of thionin. This will result in an improved selectivity and sensitivity. Third conclusion is that the TF-MGA/GNSs sensor can provide a higher sensitivity than TF-MGA-n sensor or TF-GNSs sensor, indicating that the combination of

Table 1 The comparison of electrochemical methods for the direct detection of dsDNA

Sensing materials/ analysis strategy	Linear range	Detection limit	Detection technology	Ref.
$Mo_6S_{9-x}I_x$ nanowires	6.12–73.4 ng mL^{-1}	0.62 ng mL^{-1}	Voltammetric method	[28]
Ethylendiamine-functionalized multiwalled carbon nanotubes	5–60 µg mL^{-1}	0.971 µg mL^{-1}	Voltammetry	[29]
MoS_2–thionin composite	0.09–1.9 ng mL^{-1}	0.04 ng mL^{-1}	Differential pulse voltammetry	[26]
Alkaline phosphatase conjugated to zinc finger proteins		100 fM	Voltammetry	[9]
Triplex-forming oligonucleotides		10 nM	Voltammetry	[30]
Graphite powder with 1-ethyl-3-methylimidazolium ethylsulphate and liquid paraffin.	10–600 ng mL^{-1}	1.2 ng mL^{-1}	Differential pulse voltammetry	[31]
Thionin-functionalized multiple graphene aerogel and gold nanostars	100 fg · mL^{-1}–10 ng·mL^{-1}	39 fg · mL^{-1}	Differential pulse voltammetric	Present work

Table 2 Linear range and detection limit of the sensor based on the material for detection of dsDNA

Sensing materials	Linear range (g ml^{-1})	Detection limit (g ml^{-1})	Sensing materials	Linear range (g ml^{-1})	Detection limit (g ml^{-1})
TF-MGA-1	3.2×10^{-12}–1.2×10^{-7}	9.9×10^{-13}	TF-GNSs	2.2×10^{-7}–1.0×10^{-4}	6.2×10^{-8}
TF-MGA-4	2.6×10^{-13}–2.5×10^{-8}	8.3×10^{-14}	TF-MGA-4/GNSs	1.9×10^{-13}–1.5×10^{-8}	5.7×10^{-14}
TF-MGA-8	2.0×10^{-14}–1.0×10^{-9}	6.4×10^{-15}	TF-MGA-8/GNSs	1.3×10^{-14}–1.0×10^{-9}	4.2×10^{-15}
TF-MGA-12	1.2×10^{-15}–3.2×10^{-10}	4.6×10^{-16}	TF-MGA-12/GNSs	1.2×10^{-15}–2.5×10^{-10}	3.1×10^{-16}

MGA with GNS leads to an enhanced sensitivity. During the electrode reaction, the MGA-n plays very important roles in the electro-catalytic activity to oxidation and reduction of thionin. On the one hand, the MGA-n offers a high electrical conductivity. This will enhance the electron transfer between the electrode and the electrolyte. On the other hand, the MGA-n provides a well-defined three-dimensional structure with a rich of open pores. The existence of these open holes greatly accelerates the electrolyte transport. In addition, the MGA-n also acts as a connector of GNS particles in the TF-MGA-n/ GNSs composite and increases the electrical conductivity. More importantly, the significant synergy between the MGA and the GNS will greatly improve the electro-catalytic activity of the MGA-n/ GNSs composite, thus leading to an ultra high sensitivity.

Interference study

The selectivity of the sensor over proteins was investigated to verify the practical use of the dsDNA sensor. DPV revealed a small decrease in the peak current after addition of 1 μg·mL^{-1} of BSA. This is because BSA can adsorb on the modified electrode surface due to the electrostatic interaction between negatively charged BSA and positively charged thionin, which will hinder the redox of thionin and leads to reduce the peak current. Further, we examined the response of the sensor to dsDNA in the presence of 1 μg mL^{-1} BSA. The result shows that this sensor also exhibits a good response with the addition of dsDNA at different concentration in the presence of 1 μg mL^{-1} BSA. A linear relationship between the peak current and the concentration of dsDNA from 100 fg mL^{-1} to 10 ng mL^{-1} is also obtained. The sensitivity of the DPV response to dsDNA is almost as the same as that of the sensor in the absence of BSA in the solution. The result demonstrates that the sensor is suitable for the detection of dsDNA in the presence of high concentration of BSA.

Determination of circulating free DNA in human serum

The method was used to detect the concentration of circulating free DNA in human serum. The circulating free DNA was extracted from healthy human serum and then added to the N$_2$ saturated the PBS. The circulating free DNA content in the

human serum was calculated to be 0.76 ± 0.05 ng mL^{-1}. In addition, the recoveries of this method were tested by adding 0.1 ng mL^{-1} of the dsDNA into the serum. The recovery is in the range from 95.2 to 101.4 %, indicating that the method has good accuracy and precision. Therefore, the method is applicable to the detection of the natural DNA in real samples.

Conclusions

The study demonstrates the synthesis of thionin-functionalized multiple graphene aerogel/gold nanostars composite and its application as sensing material for the electrochemical detection od DNA. The result shows that the multiple graphene aerogel gives a much better electrochemical behaviour compared to the classical graphene aerogel. The hybridization of multiple graphene aerogel with gold nanostars achieves a significantly electrochemical synergy, thus leading to an enhanced the electrochemical response to DNA. The biosensor based on the composite exhibits a higher sensitivity than that of other sensors reported in literatures. The study also provides an attractive approach for building graphene aerogel-based materials to meet the needs of nanoelectronics for molecular diagnosis, bioanalysis and catalysis.

Compliance with ethical standards The author(s) declare that they have no competing interests.

References

1. Sullivan I, Salazar J, Majem M, Pallares C, del Rio E, Paez D, Baiget M, Barnadas A (2014) Pharmacogenetics of the DNA repair pathways in advanced non-small cell lung cancer patients treated with platinum-based chemotherapy. Cancer Lett 353:160–166
2. Harrington R, Datta V, Camalier C, Walsh W, Sims D, Das B, Lih C, Williams P (2014) Comparison of spectrophotometry and qPCR for determining dna concentration from FFPE samples for next-generation sequencing assay. J Mol Diagn 16:773

3. Huang HH, Yang XH, Wang KM, Wang G, Guo QP, Huang J, Liu JB, Guo XC, Li WS, He LL (2015) Amplified fluorescence detection of DNA based on catalyzed dynamic assembly and host-guest interaction between beta-cyclodextrin polymer and pyrene. Talanta 144:529–534

4. Duan B, Zhou JJ, Fang Z, Wang CX, Wang XJ, Hemond HF, Chan-Park MB, Duan HW (2015) Surface enhanced Raman scattering by graphene-nanosheet-gapped plasmonic nanoparticle arrays for multiplexed DNA detection. Nanoscale 7:12606–12613

5. Bonvicini F, Mirasoli M, Zangheri M, Nascetti A, De Cesare G, Caputo D, Roda A, Gallinella G (2015) Detection of viral DNA by isothermal NASBA amplification and chemiluminescence gene probe hybridization assay in a microfluidic cartridge. J Clin Virol 70:S91–S92

6. Das R, Goel AK, Sharma MK, Upadhyay S (2015) Electrochemical DNA sensor for anthrax toxin activator gene atxA-detection of PCR amplicons. Biosens Bioelectron 74:939–946

7. Yang YZ, Gao F, Cai XL, Yuan XN, He SY, Gao F, Guo HX, Wang QX (2015) beta-Cyclodextrin functionalized graphene as a highly conductive and multi-site platform for DNA immobilization and ultrasensitive sensing detection. Biosens Bioelectron 74:447–453

8. Rachel W, Nirmal G, Priscila B, Elissa G, Krisanu B (2015) Mediated electron transfer at vertically aligned single-walled carbon nanotube electrodes during detection of DNA hybridization. Nanoscale Res Lett 10:978–982

9. Li ZB, Miao XM, Xing K, Zhu AH, Ling LS (2015) Enhanced electrochemical recognition of double-stranded DNA by using hybridization chain reaction and positively charged gold nanoparticles. Biosens Bioelectron 74:687–690

10. Noh S, Ha DT, Yang H, Kim MS (2015) Sensitive and direct electrochemical detection of double-stranded DNA utilizing alkaline phosphatase-labelled zinc finger proteins. Analyst 140:3947–3952

11. Liu HL, Fang GZ, Deng QL, Wang S (2015) A triple-dimensional sensing chip for discrimination of eight antioxidants based on quantum dots and graphene. Biosens Bioelectron 74:313–317

12. Chao HW, Liao WP, Lin WH, Yoshimura M, Wu JJ (2015) Pristine reduced graphene oxide as an energy-matched auxiliary electron acceptor in nanoarchitectural metal oxide/poly(3-hexylthiophene) hybrid solar cell. J Power Sources 293:246–252

13. Wu K, Zhang Q, Sun DM, Zhu XS, Chen Y, Lu TH, Tang YW (2015) Graphene-supported Pd-Pt alloy nanoflowers: in situ growth and their enhanced electrocatalysis towards methanol oxidation. Int J Hydrog Energy 40:6530–6537

14. Wu GH, Li RY, Li ZJ, Liu JK, Gu ZG, Wang GL (2015) N-doped graphene/graphite composite as a conductive agent-free anode material for lithium ion batteries with greatly enhanced electrochemical performance. Electrochim Acta 171:156–164

15. Li RY, Jiang YY, Zhou XY, Li ZJ, Gu ZG, Wang GL, Liu JK (2015) Significantly enhanced electrochemical performance of lithium titanate anode for lithium ion battery by the hybrid of nitrogen and sulfur co-doped graphene quantum dots. Electrochim Acta 178:303–311

16. Nardecchia S, Carriazo D, Ferrer ML, Gutierrez MC, Monte FD (2013) Three dimensional macroporous architectures and aerogels built of carbon nanotubes and/or graphene: synthesis and applications. Chem Soc Rev 42:794–830

17. Yu ZN, Mclnnis M, Calderon J, Seal S, Zhai L, Thomas J (2015) Functionalized graphene aerogel composites for high-performance asymmetric supercapacitors. Nano Energy 11:611–620

18. Zhang JJ, Li RY, Li ZJ, Liu JK, Gu ZG, Wang GL (2014) Synthesis of nitrogen-doped activated graphene aerogel/gold nanoparticles and its application for electrochemical detection of hydroquinone and o-dihydroxybenzene. Nanoscale 6:5458–5466

19. Wang M, Wang JZ, Hou YY, Shi DQ, Wexler D, Poynton SD, Slade RCT, Zhang WM, Liu HK, Chen J (2015) N-doped crumpled graphene derived from vapor phase deposition of PPy on graphene aerogel as an efficient oxygen reduction reaction electrocatalyst. ACS Appl Mater Interfaces 7:7066–7072

20. Meng JK, Cao Y, Suo Y, Liu YS, Zhang JM, Zheng XC (2015) Facile Fabrication of 3D SiO_2@graphene aerogel composites as anode material for lithium ion batteries. Electrochim Acta 176:1001–1009

21. Wu WJ, Wan CY, Zhang Y (2015) Graphene oxide as a covalent-crosslinking agent for EVM-g-PA6 thermoplastic elastomeric nano-composites. RSC Adv 5:39042–39051

22. Xu J, Wang DX, Yuan Y, Wei W, Duan LL, Wang LX, Bao HF, Xu WL (2015) Polypyrrole/reduced graphene oxide coated fabric electrodes for supercapacitor application. Org Electron 24:153–159

23. Ramasamy MS, Mahapatra SS, Cho JW (2015) Functionalization of graphene with self-doped conducting polypyrrole by click coupling. J Colloid Interface Sci 455:63–70

24. Hummers WS, Offeman RE (1958) Preparation of graphitic oxide. J Am Chem Soc 80:1339

25. Gao LB, Ren WC, Xu HL, Jin L, Wang ZX, Ma T, Ma LP, Zhang ZY, Fu Q, Peng LM, Bao XH, Cheng HM (2012) Repeated growth and bubbling transfer of graphene with millimetre-size single-crystal grains using platinum. Nat Commun 3:699-1–699-7

26. Wang TY, Zhu RZ, Zhuo JQ, Zhu ZW, Shao YH, Li MX (2014) Direct detection of DNA below ppb level based on thionin-functionalized layered MoS_2 electrochemical sensors. Anal Chem 86:12064–12069

27. Abdul Rashid JI, Yusof NA, Abdullah J, Hashim U, Hajian R (2014) The utilization of SiNWs/ AuNPs-modified indium tin oxide (ITO) in fabrication of electrochemical DNA sensor. Mater Sci Eng C 45:270–276

28. Lin H, Cheng HM, Liu L, Zhu ZW, Shao YH, Papakonstantinou P, Mihailovic D, Li MX (2011) Thionin attached to a gold electrode modified with self-assembly of $Mo_6S_{9-X}I_X$ nanowires for amplified electrochemical detection of natural DNA. Biosens Bioelectron 26:1866–1870

29. Caete-Rosales P, Alvarez-Lueje A, Bollo S (2014) Ethylendiamine-functionalized multi-walled carbon nanotubes prevent cationic dispersant use in the electrochemical detection of dsDNA. Sensors Actuators B Chem 191:688–694

30. Patterson A, Caprio F, Vallee-Belisle A, Moscone D, Plaxco KW, Palleschi G, Ricci F (2010) Using triplex-forming oligonucleotide probes for the reagentless, electrochemical detection of double-stranded DNA. Anal Chem 82:9109–9115

31. Zhu ZH, Li X, Zeng Y, Sun W (2010) Ordered mesoporous carbon modified carbon ionic liquid electrode for the electrochemical detection of double-stranded DNA. Biosens Bioelectron 25:2313–2317